Int. J. Heat Mass Transfer. Vol. 28, No. 6, pp. 1067–1088, 1985
Printed in Great Britain

0017–9310/85 $3.00 + 0.00

Turbulence modeling in combined convection in mercury pipe flow

MARCELO J. S. de LEMOS*
Mechanical Engineering Department—PUC/RJ, Rio de Janeiro, 22453 Brazil

and

ALEXANDER SESONSKE
Purdue University, West Lafayette, IN 47907, U.S.A.

(*Recieved* 14 *May* 1984 *and in final form* 2 *November* 1984)

Abstract—A simplified Algebraic Stress Model was used to investigate the effect of buoyancy on the mean and turbulent flow of mercury in a pipe. The Patankar and Spalding finite difference method was used for solving the governing parabolic flow equations. Results were compared with previous measurements covering a Ra/Re^2 range from near zero to 10^{-4} for $30{,}000 < Re < 90{,}000$ and qualitatively predicted observed distortions. Temperature fluctuations were measured to supplement previous experiments in the near-wall region. Heating effects on turbulent energy and momentum transfer were predicted. Modeling also confirmed measured reversal of the turbulent axial flux.

INTRODUCTION

IN ANY flow system, a body force acts in a fluid element in addition to surface forces. This action is primarily dependent upon the flow orientation in relation to the gravitational field.

When the flow is turbulent, gravitational forces are present in the mean and turbulent fields. Depending on certain flow parameters, this influence can be predominant in one of them or equally important in both fields. Experimental evidence gathered in the last 15 years has shown substantial distortion in the fluctuating and time-averaged flows due to action of buoyancy forces. These distortions cause significant variations in the overall coefficients of momentum and heat transfer [1].

It has been established [2, 3] that in buoyancy-affected turbulent flow in vertical pipes, as a consequence of increasing the wall heat load, the modeling of the turbulent kinetic energy is required to well represent the important features occurring in the measured heat transfer coefficients.

The turbulent kinetic energy equation written for a simple two-dimensional (2-D) shear layer in a system oriented in the upward direction shows an extra term representing the direct influence of buoyancy in the turbulence, $(\beta g/T)\overline{u\theta}$, where $\overline{u\theta}$ is in the axial direction. Also, the radial turbulent momentum and heat transport terms appearing in the time-averaged equations involve the correlations $\overline{uv}$ and $\overline{v\theta}$.

In order to mathematically close the set of equations which will be shown later, there is a need for a model for $\overline{uv}$, $\overline{v\theta}$, and $\overline{u\theta}$.

Among possible closures, the eddy diffusivity models give the correlations,

$$-\overline{uv} = \nu_t \frac{\partial U}{\partial y} \tag{1}$$

$$-\overline{v\theta} = \alpha_t \frac{\partial T}{\partial y} \tag{2}$$

and

$$-\overline{u\theta} = \alpha_t \frac{\partial T}{\partial x} \tag{3}$$

where y is the radial direction and x is in the upward axial direction.

By means of equations (1) and (2), calculated values for the eddy diffusivities, ν_t and α_t, using measured distorted radial profiles for the mean velocity and mean temperature, led to the observation that eddy diffusivities were very sensitive to heat fluxes [4, 5, 6, 7]. Therefore, Jacoby *et al.* [7] concluded that this concept appeared to be of limited usefulness for generalized heat transfer modeling, at least in mercury at the conditions studied.

A more important aspect of the limitation of the eddy diffusivity concept for the prediction of the turbulence structure for the flow under consideration can be seen by means of equation (3). For an upward heated flow (temperature increasing with height), the use of (3) gives a downward direction (negative value) for the axial heat flux $\rho c_p \overline{u\theta}$. The experiments of Carr *et al.* [8], Hochreiter [9] and Flaherty [10] show a substantial change in the turbulence structure under the effect of buoyancy implying the *reversal* of the direction of the axial turbulent heat flux. This drastic change in the flow transport properties *cannot* be calculated by the model of equation (3).

The present contribution numerically investigates the effect of buoyancy on the mean *and* turbulent fields for a heated vertical upward flow of mercury. The

* Presently on leave at Components Technology Division, Argonne National Laboratory, Argonne, IL 60439, U.S.A.

NOMENCLATURE

A axial temperature gradient, $\partial T/\partial x$

c model constants

c_p specific heat at constant pressure

D pipe diameter

$\mathscr{D}_\xi$ diffusion term of ϕ in the ϕ transport equation, $\phi = \overline{u_i u_j}$, $\overline{u_j\theta}$, k, ε or g and $\xi = ij, j\theta, k, \varepsilon$ and g, respectively.

f wall effect function, $\dfrac{k^{3/2}}{c_w \varepsilon x_n}$; Fanning friction factor

G generation rate of turbulent energy due to buoyancy effects, $\dfrac{\overline{\rho' u_i} g_i}{\rho} = \dfrac{-\beta \overline{u_i\theta} g_i}{T}$

G_{ij} kinematic production rate of $\overline{u_i u_j}$ by buoyancy forces, $\dfrac{\overline{\rho' u_i} g_j}{\rho} + \dfrac{\overline{\rho' u_j} g_i}{\rho} = -\dfrac{\beta}{T}(\overline{u_i\theta} g_j + \overline{u_j\theta} g_i)$

$G_{j\theta}$ kinematic production rate of $\overline{u_j\theta}$ due to buoyancy effects, $\dfrac{\overline{\rho'\theta} g_j}{\rho} = \dfrac{-\beta\overline{\theta^2} g_j}{T}$

Gr_A Grashof number based on axial temperature gradient, $\rho_b^2 \beta g A D^4/\mu^2$

g $\overline{\theta^2}/2$

g_i gravitation acceleration in the x_i direction

k turbulent kinetic energy, $\overline{u_i u_i}/2$

l turbulence length scale, $k^{3/2}/\varepsilon$

P mean static pressure, $-\overline{u_i u_k}\dfrac{\delta U_i}{\delta x_k}$ = generation rate of turbulence energy due to mean velocity gradients

Pe Peclet number, $RePr$

Pe_t turbulent Peclet number, $Re_t Pr = k^2/\varepsilon\alpha$

P_g generation rate of g by mean temperature gradients, $-\overline{u_k\theta}\dfrac{\partial T}{\partial x_k}$

P_{ij} kinematic production rate of $\overline{u_i u_j}$ by mean velocity gradients, $-\left(\overline{u_i u_k}\dfrac{\partial U_j}{\partial x_k} + \overline{u_j u_k}\dfrac{\partial U_i}{\partial x_k}\right)$

$P_{j\theta}$ kinematic production rate of $\overline{u_j\theta}$ by mean velocity gradients, $-\overline{u_k\theta}\dfrac{\partial U_j}{\partial x_k}$

Pr Prandtl number, $\mu c_p/\lambda$

R ratio of time scales of turbulent temperature and velocity fields, $\dfrac{\varepsilon g}{k\varepsilon_g}$; pipe radius

Ra Rayleigh number, $\rho_b^2 \beta g c_p A D^4/\mu\lambda = PrGr_A$

Re Reynolds number, DU_b/ν

Re_t turbulent Reynolds number, $\dfrac{lk^{1/2}}{\nu} = \dfrac{k^2}{\nu\varepsilon}$

T mean temperature

T^* friction temperature, $q_w/\rho c_p U^*$

T^+ dimensionless temperature, T/T^*

U^* friction velocity, $U_b\sqrt{f/2}$

U^+ dimensionless velocity, U/U^*

U_i mean velocity in the x_i direction

u_i fluctuating velocity component in x_i direction

$\overline{u_i u_j}$ kinematic Reynolds stress

$\overline{u_j\theta}$ turbulent flux of heat divided by ρc_p

x_i Cartesian-space coordinate (tensor suffix notation)

y distance from wall

y^+ dimensionless wall coordinate, yU^*/ν.

Greek symbols

α thermal diffusivity, $\dfrac{\lambda}{\rho c_p}$

β dimensionless volumetric expansion coefficient, $-\dfrac{\partial\rho}{\partial t}\Big|_p \dfrac{T}{\rho}$

ε kinematic dissipation rate of turbulent kinetic energy

ε_g kinematic dissipation rate of variance of temperature fluctuations

$\varepsilon_{j\theta}$ dissipation rate of $\overline{u_j\theta}$

ε_{ij} dissipation rate of $\overline{u_i u_j}$

θ fluctuating temperature

$\overline{\theta^2}$ variance of temperature fluctuations

λ thermal conductivity

μ molecular dynamic viscosity

π_{ij} pressure–strain correlation (general), $\overline{\dfrac{p}{\rho}\left(\dfrac{\partial u_i}{\partial x_j} + \dfrac{\partial u_i}{\partial x_i}\right)}$

$\pi_{ij,1}$ first part of π_{ij}, associated with turbulence–velocity interactions, $-c_1\dfrac{\varepsilon}{k}(\overline{u_i u_j} - \frac{2}{3}\delta_{ij}k)$

$\pi_{ij,2}$ second part of π_{ij}, associated with mean strain, $-c_2(P_{ij} - \frac{2}{3}\delta_{ij}P)$

$\pi_{ij,3}$ third part of π_{ij}, associated with buoyancy, $-c_3(G_{ij} - \frac{2}{3}\delta_{ij}G)$

$\pi_{j\theta}$ pressure–temperature gradient correlation (general), $\overline{\dfrac{p}{\rho}\dfrac{\partial\theta}{\partial x_j}}$

$\pi_{j\theta,1}$ turbulence part of $\pi_{j\theta}$, $-c_{1\theta}\dfrac{\varepsilon}{k}\overline{u_j\theta}$

$\pi_{j\theta,2}$ mean strain part of $\pi_{j\theta}$, $-c_{2\theta}P_{j\theta}$

$\pi_{j\theta,3}$ buoyancy part of $\pi_{j\theta}$, $-c_{3\theta}G_{j\theta}$

ρ density

ρ' fluctuations in density about mean (included in buoyant terms only)

σ_ξ	turbulent Prandtl number for T, k, ε and g when $\xi = t$, k, ε and g, respectively	Subscripts	
		t	turbulent value
τ	shear stress	w	wall value
ν	kinematic viscosity.	b	bulk value.

approach used here does not make use of the eddy diffusivity concept which, according to the foregoing, seems to be of limited usefulness at least for the class of flow under consideration.

MATHEMATICAL MODEL

In this section, the transport equations for the mean velocity and temperature and for the turbulent stresses/fluxes are presented together with the closure assumptions used. Also presented are equations for k, ε and $g = \overline{\theta^2}/2$, as required for closing the system of equations. The basic difference from the model presented here and the second-order closures published in the literature is the treatment of certain terms in the $\overline{u_j\theta}$ and g equations which are assumed here as dependent upon Pr. Predictive relations are proposed for liquid metal flows and asymptotic behavior for $Pr \sim 1$ cases is also accounted for.

The time-averaged momentum and energy equations for subsonic incompressible flow can be written as,

$$\rho\frac{DU_i}{Dt} = -\frac{\partial P}{\partial x_i} + \frac{\partial}{\partial x_j}\left[\mu\left(\frac{\partial U_i}{\partial x_j} + \frac{\partial U_j}{\partial x_i}\right) + \overline{-u_iu_j}\right] + \rho g_i \tag{4}$$

$$\rho c_p\frac{DT}{Dt} = \frac{\partial}{\partial x_j}\left(\lambda\frac{\partial T}{\partial x_j} - \rho c_p\overline{u_j\theta}\right). \tag{5}$$

The correlations $\overline{u_iu_j}$ and $\overline{u_j\theta}$ appearing in the RHS of equations (4) and (5), respectively, represent two additional unknowns in the problem of solving the velocity and thermal fields. These extra terms are a consequence of the averaging process over the convective term.

An exact equation for the Reynolds stresses, $\rho\overline{u_iu_j}$, can be derived by multiplying the x_i-component of the instantaneous case of equation (4) by u_j and adding u_i multiplied by the x_j-component of the same equation. Then time averaging.

The modeled form of the $\overline{u_iu_j}$ equation used here comes mainly from refs. [11] and [12]. Since in this work no novelty was introduced in closing the hydrodynamic field, the details of modeling the $\overline{u_iu_j}$ equation can be found in the above references. Here it is sufficient to say that the final form for the $\overline{u_iu_j}$ equation is,

$$\frac{D\overline{u_iu_j}}{Dt} = P_{ij} + G_{ij} + \pi_{ij,1} + \pi_{ij,2} + \pi_{ij,3} + \pi_{ij,w} - \tfrac{2}{3}\delta_{ij}\varepsilon + \mathscr{D}_{ij} \tag{6}$$

where P_{ij} and G_{ij} are the production of $\overline{u_iu_j}$ by mean flow and buoyancy, respectively, $\pi_{ij,1}$, $\pi_{ij,2}$, and $\pi_{ij,3}$ are the turbulent, mean flow and buoyant parts of π_{ij}, $\pi_{ij,w}$ is a wall correction to π_{ij}, and ε is the dissipation of turbulent kinetic energy. The diffusion term, $\mathscr{D}_{ij}$, is the same as in the exact $\overline{u_iu_j}$ equation since models for transport terms are not necessary, as will be seen later.

Modeled equations for k and ε are derived in the literature [13, 14] and will be just presented here. The transport of k along a streamline is governed by,

$$\frac{Dk}{Dt} = P + G - \varepsilon + \mathscr{D}_k \tag{7}$$

where

$$\mathscr{D}_k = \frac{\partial}{\partial x_j}\left[\frac{\nu_t}{\sigma_k}\frac{\partial k}{\partial x_j}\right]$$

is based upon the gradient transport assumption, and P and G are production of turbulent kinetic energy by mean flow and buoyancy, respectively. For ε, the transport equation reads,

$$\frac{D\varepsilon}{Dt} = c_{\varepsilon 1}\frac{\varepsilon}{k}P + c_{\varepsilon 3}\frac{\varepsilon}{k}G - c_{\varepsilon 2}\frac{\varepsilon^2}{k} + \mathscr{D}_\varepsilon \tag{8}$$

where

$$\mathscr{D}_\varepsilon = \frac{\partial}{\partial x_j}\left[\frac{\nu_t}{\sigma_\varepsilon}\frac{\partial \varepsilon}{\partial x_k}\right].$$

In equations (7) and (8) the cs and σs are constants to be presented later.

For the turbulent heat fluxes, an exact transport equation can be obtained using a procedure similar to the one used to obtain the $\overline{u_iu_j}$-equation. The result reads [15],

$$\frac{D\overline{u_j\theta}}{Dt} = -\overline{u_ju_k}\frac{\partial T}{\partial x_k} + P_{j\theta} + G_{j\theta} + \pi_{j\theta} + \varepsilon_{j\theta} + \mathscr{D}_{j\theta} \tag{9}$$

where,

$$P_{j\theta} = -\overline{u_k\theta}\frac{\partial U_j}{\partial x_k}, \quad G_{j\theta} = \frac{\overline{\rho'\theta}g_j}{\rho}$$

$$\varepsilon_{j\theta} = \nu\overline{\frac{\partial\theta}{\partial x_k}\left(\frac{\partial u_j}{\partial x_k} + \frac{\partial u_k}{\partial x_j}\right)} + \frac{\lambda}{\rho c_p}\overline{\frac{\partial\theta}{\partial x_k}\frac{\partial u_j}{\partial x_k}}; \quad \pi_{j\theta} = \overline{\frac{p}{\rho}\frac{\partial\theta}{\partial x_j}}$$

$$\mathscr{D}_{j\theta} = \frac{\partial}{\partial x_k}\left[-\overline{\rho u_ku_j\theta} + \frac{\lambda}{c_p}\overline{u_j\frac{\partial\theta}{\partial x_k}} + \mu\overline{\theta\left(\frac{\partial u_j}{\partial x_k} + \frac{\partial u_k}{\partial x_j}\right)} - \overline{p\theta}\,\delta_{jk}\right].$$

Equation (9) is valid for liquids and when compressible effects and viscous production are negligible. Inspecting (9) one sees that the last three terms on the RHS need modeling. Here, attention is focused to liquid metals and prognostic relations with dependence on Pr are suggested.

For high Reynolds number, $\varepsilon_{j\theta}$ can be written as [16],

$$\varepsilon_{j\theta} = (\alpha+\nu)\overline{\frac{\partial u_j}{\partial x_k}\frac{\partial \theta}{\partial x_k}} \tag{10}$$

where

$$\alpha = \frac{\lambda}{\rho c_p}.$$

Lumley and his co-workers [17, 18], as well as Launder [19], assume that equation (10) is negligible when local isotropy also prevails in the thermal field, or,

$$\left[\overline{\left(\frac{\partial\theta}{\partial x}\right)^2}\right]^{1/2} = \left[\overline{\left(\frac{\partial\theta}{\partial y}\right)^2}\right]^{1/2} = \left[\overline{\left(\frac{\partial\theta}{\partial z}\right)^2}\right]^{1/2}. \tag{11}$$

Gibson [16] points out that under this condition it is the randomizing action of the pressure–temperature gradient correlation which limits the growth of fluxes $\overline{u_j\theta}$.

However, for liquid metals, equation (11) is not expected to hold, since even the smallest eddies are themselves influenced by action of the high thermal conductivity. This is consistent with the reasoning involved in many previous works in liquid metals (see for example [20]).

In approximating (10), one should get the correct asymptotic behavior when $Pr \sim 1$ and Re_t is large, or let us say, $\varepsilon_{j\theta}$ should attain very small values under these conditions. With this idea in mind, and using an order of magnitude argument similar to the one presented by Tennekes and Lumley [21], $\partial u_j/\partial x_k$ can be approximated as,

$$\overline{\frac{\partial u_j}{\partial x_k}} \sim \frac{k^{1/2}}{l} \tag{12}$$

where k is the turbulent kinetic energy and l a turbulence length scale. Similarly $\partial\theta/\partial x_j$ is assumed as,

$$\overline{\frac{\partial \theta}{\partial x_k}} \sim \frac{g^{1/2}}{l_\theta} \tag{13}$$

where $g = \overline{\theta^2}/2$ is one half of the variance of temperature fluctuations and l_θ is a length scale associated with the thermal field. The quantities $k^{1/2}$ and $g^{1/2}$ are representatives of velocity and scalar scales, respectively, for the energy containing eddies. Thus using equations (12) and (13),

$$\varepsilon_{j\theta} \sim \left(1+\frac{1}{Pr}\right)\nu\frac{k^{1/2}g^{1/2}}{l\,l_\theta}. \tag{14}$$

Furthermore, one can assume [21],

$$k^{1/2}g^{1/2} \sim \overline{u_j\theta}$$

and noting that,

$$\frac{\nu}{l^2} = \frac{1}{Re_t}\frac{\varepsilon}{k}$$

(14) becomes,

$$\varepsilon_{j\theta} \sim \left(1+\frac{1}{Pr}\right)\frac{1}{Re_t(l_\theta/l)}\frac{\varepsilon}{k}\overline{u_j\theta}. \tag{15}$$

As mentioned before, the asymptotic behavior $\varepsilon_{j\theta} \to \infty$ for $Pr \sim 1$ is retained in equation (15).

In deriving (15), the ratio of length scales l_θ/l is introduced. Since the model works with only *one* length scale, the ratio of length scales has to be supplied. By using available experimental data on energy containing length scales for several Prandtl numbers, one has,

$$\frac{l_\theta}{l} = 0.821\ Pr^{-0.2} + \frac{0.179}{Pr^{0.5}}. \tag{16}$$

The above relation was obtained by curve fitting the results of refs. [9, 22, 23, 24] for l_θ and l, which were obtained through spectral analysis. Equation (15) is now calculable, once k and ε are available. The proportionality factor in (15) is taken as $c_{1\theta}/c_{j\theta}$, where the cs are constants to be determined later.

As with the pressure–strain correlation π_{ij} in equation (6), $\pi_{j\theta}$ in equation (9) can be split as,

$$\pi_{j\theta} = \pi_{j\theta,1} + \pi_{j\theta,2} + \pi_{j\theta,3} \tag{17}$$

where $\pi_{j\theta,1}$ is the 'turbulent interaction' part of $\pi_{j\theta}$, and $\pi_{j\theta,2}$ and $\pi_{j\theta,3}$ can be interpreted as the decreasing of production rates by shear and buoyancy, respectively, caused by pressure fluctuations. The last two terms are modeled exactly as in ref. [11] where more details can be found.

To model the first part, $\pi_{j\theta,1}$, the view of Monin [25] is adopted here as

$$\pi_{j\theta,1} = -c_{1\theta}\frac{\varepsilon}{k}\overline{u_j\theta}. \tag{18}$$

The two terms, $\varepsilon_{j\theta}$ and $\pi_{j\theta,1}$, can be combined as,

$$\varepsilon_{j\theta} + \pi_{j\theta,1} = -c_{1\theta}\frac{\varepsilon}{k}F_1\overline{u_j\theta} \tag{19}$$

where

$$F_1 = \left[1+\left(1+\frac{1}{Pr}\right)\frac{1}{c_{j\theta}\,Re_t(l_\theta/l)}\right]. \tag{20}$$

The presence of the wall is accounted for by adding an extra term. The wall correction is also as in Ljuboja and Rodi [11], but includes the functional F_1, as suggested by ref. [15],

$$\pi_{j\theta,w} = \left[-F_1\frac{\varepsilon}{k}c'_{1\theta}\overline{u_k\theta}\,n_k n_j\right]f\left(\frac{l}{x_n}\right) \tag{21}$$

where f is a function which decreases this correction for points x_n far from the wall. In addition, in the argument of f, l is a turbulence length scale and n is a unit vector perpendicular to the wall. Again, no proposal is made for $\mathscr{D}_{j\theta}$ since the difference $[(\mathrm{D}\overline{u_j\theta}/\mathrm{D}t) - \mathscr{D}_{j\theta}]$ will be neglected by model assumption. So, the final modeled form for the $\overline{u_j\theta}$ equation is,

$$\frac{\mathrm{D}\overline{u_j\theta}}{\mathrm{D}t} = -\overline{u_iu_k}\frac{\partial T}{\partial x_k} + P_{j\theta} + G_{j\theta} - c_{1\theta}\frac{\varepsilon}{k}\overline{u_j\theta}F_1 + \pi_{j\theta,2} + \pi_{j\theta,3} + \pi_{j\theta,w} + \mathscr{D}_{j\theta}. \tag{22}$$

An equation which describes the history of the

temperature fluctuations can be obtained as

$$\frac{Dg}{Dt} = P_g - \varepsilon_g + \frac{\partial}{\partial x_j}\left[\alpha\frac{\partial g}{\partial x_j} - \frac{\overline{u_j\theta^2}}{2}\right]. \quad (23)$$

Equation (23) is much the same form as the exact turbulent kinetic energy equation but the lack of perfect analogy shows up in the absence of a term corresponding to the pressure–velocity correlation.

On seeking a modeled form for (23), one should use the same reasoning embodied in modeling $\varepsilon_{j\theta}$, where only a few terms in the equation are assumed to be affected by molecular 'smearing' of the large-scale motion. Or, say, in the particular case of (23), only the dissipative and the turbulent diffusion terms are assumed to be different when Pr is of a low value. This is certainly a simplification, but at first seems to be a cautious path. Also, the modeled form shall approach asymptotic values when $Pr = 1$.

With the above ideas in mind and using a similar argument as [26], it is suggested that temperature fluctuation disappears by two mechanisms: (a) the decay of velocity field drives the decay of the temperature field in a cascade process occurring at a rate characteristic of the inertial subrange, and equal to ε/k, and (b) at the same time, heat is lost due to the fluid thermal conductivity and differences of the instantaneous temperature within the fluid. The latter mechanism is therefore much like a conduction process, and occurs at a rate proportional to α/l_θ^2, which is a characteristic rate of a diffusive transport.

Thus, assuming that the two processes are independent, or that nonlinear effects are neglected, the dissipative term can be written as,

$$\varepsilon_g = \left[\frac{\alpha}{c_g l_\theta^2} + \frac{1}{c'}\frac{\varepsilon}{k}\right] g, \quad (24)$$

but noting that

$$\frac{\alpha}{l^2} = \frac{1}{Pe_t}\frac{\varepsilon}{k}$$

and taking

$$c' = R_\infty$$

where R_∞ is the limiting time scale ratio R, when $Pe_t \gg 1$, equation (24) is

$$\varepsilon_g = \frac{\varepsilon}{kR} g \quad (25)$$

where

$$R = \left[\frac{1}{c_g Pe_t (l_\theta/l)^2} + \frac{1}{R_\infty}\right]^{-1}. \quad (26)$$

It is seen in equation (26) that for

$$Pe_t \to \infty; \quad \varepsilon_g = \frac{\varepsilon}{kR_\infty} g \quad (27)$$

or only that mechanism (a) is important. Equation (27) is usually used in the literature to represent ε_g. The ratio (l_θ/l) is calculated from (18) and c_g shall be determined later. Equation (26) is calculable once k, ε, and g become available.

The last term on the RHS of (23) is approximated using once again the gradient transport notion. Therefore, the turbulent diffusion term is assumed as,

$$\frac{\partial}{\partial x_j}\left(-\frac{\overline{u_j\theta^2}}{2}\right) = \frac{\partial}{\partial x_j}\frac{Rv_t}{\sigma_g}\frac{\partial g}{\partial x_j}. \quad (28)$$

In (28) the inclusion of R indicates the contribution of the thermal field time scale in transporting temperature fluctuations, see ref. [15]. The constant σ_g shall be determined later.

The final modeled form for (23) is then,

$$\frac{Dg}{Dt} = P_g - \frac{\varepsilon g}{kR} + \frac{\partial}{\partial x_j}\left[\alpha + \frac{Rv_t}{\sigma_g}\right]\frac{\partial g}{\partial x_j}. \quad (29)$$

The task of solving the flow and thermal fields, using (4), (5), (6) and (22) requires for the general 3-D case the solution of a system of 13 transport equations. In order to reduce the number of turbulence transport equations, and still keep the same information as in (6) and (22), Rodi [27] suggests that the transport terms in the Reynolds stress equation can be considered as proportional to the transport of k,

$$\frac{D\overline{u_iu_j}}{Dt} - \mathscr{D}_{ij} = \frac{\overline{u_iu_j}}{k}\left(\frac{Dk}{Dt} - \mathscr{D}_k\right). \quad (30)$$

To derive equations applicable to pipe flow, the scheme presented by Ljuboja and Rodi [12] is used. For the stress component $\overline{uv}$ and for the heat flux correlations $\overline{u\theta}$ and $\overline{v\theta}$, a local equilibrium assumption

$$\text{Conv.} - \text{Diff.} = 0 \quad (31)$$

is applied. The coordinate system is based on Fig. 1 and details on the derivation are presented in ref. [28].

The final set of equations is,

$$-\overline{uv} = w\frac{\overline{v^2}}{k}\frac{k^2}{\varepsilon}\frac{\partial U}{\partial y} \quad (32)$$

where,

$$w = \left[\frac{(1-c_2+c_2'c_2\tfrac{3}{2}f) + \dfrac{(1-c_3)B}{F_1(c_{1\theta}+c_{1\theta}'f)}}{(c_1+\tfrac{3}{2}c_1'f)}\right] \quad (33)$$

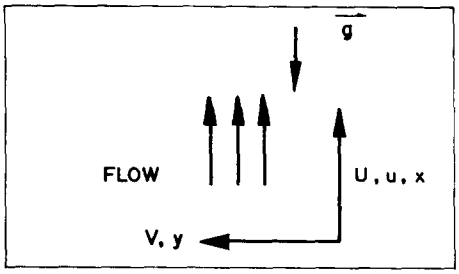

FIG. 1.

and

$$B = \frac{\beta}{T} g_x \frac{k}{\varepsilon} \frac{\partial T}{\partial y} \Big/ \partial U/\partial y \tag{34}$$

$$\frac{\overline{v^2}}{k} = \frac{2}{3}\left[\frac{c_1 - 1 + \dfrac{P+G}{\varepsilon}(c_2 - c_2 c_2' f) + \dfrac{G}{\varepsilon}(c_3 - c_2 + c_2 c_2' f)}{c_1 + \dfrac{P+G}{\varepsilon} - 1 + 2c_1' f}\right]. \tag{35}$$

For the thermal field, the equations read,

$$-\overline{v\theta} = \frac{\dfrac{k^2}{\varepsilon}\dfrac{\overline{v^2}}{k}\dfrac{\partial T}{\partial y}}{F_1(c_{1\theta} + c_{1\theta}' f)} \tag{36}$$

and

$$-\overline{u\theta} = \frac{1}{c_{1\theta} F_1}\frac{k}{\varepsilon} \times \left[\overline{uv}\frac{\partial T}{\partial y} + (1 - c_{2\theta})\overline{v\theta}\frac{\partial U}{\partial y} - \beta g_x (1 - c_{3\theta}) 2g\right]. \tag{37}$$

The turbulent Prandtl number, σ_t, is obtained from (32) and (36) as,

$$\sigma_t = w(c_{1\theta} + c_{1\theta}' f) F_1 \tag{38}$$

where w is defined in (33), and F_1 given by (20).

By inspecting the system of equations for U (4), T (5), k (7), ε (8) and g (29), and algebraic relations for $\overline{uv}$ (32), $\overline{v^2}$ (35), $\overline{v\theta}$ (36) and $\overline{u\theta}$ (37), one can see that the problem is mathematically closed.

BOUNDARY CONDITIONS

At the pipe centerline, the derivatives of the mean and turbulence quantities are taken as zero, or

$$\left.\frac{\partial \phi}{\partial y}\right|_{y=R} = 0 \tag{39}$$

where ϕ stands for U, T, k, ε and g.

In the region near the wall, the proposed model is not applied to the viscous sublayer. Therefore, for the velocity U, one assumes that at the junction point, defined as the point located sufficiently far from the wall so that molecular exchange is now totally overwhelmed by turbulent mixing, there is a region where the velocity is related to the friction velocity, $U^* = (\tau_w/\rho)^{1/2}$, via the logarithmic law of the wall, as in ref. [13],

$$U^+ = \frac{1}{\kappa} \ln (y^+ E) \tag{40}$$

where $U^+ = U/U^*$, $y^+ = yU^*/\nu$, $\kappa = 0.435$ is the von Karman constant, and $E = 9.0$ for smooth walls. These values were taken from Patankar and Spalding [29].

In the above given y-region, production and dissipation of turbulent kinetic energy are in balance. This assumption, together with the Kolmogorov–Prandtl expression, $\mu_t = \rho c_\mu k^2/\varepsilon$, gives for k at the junction point [13],

$$k = U^{*2} c_\mu^{1/2}. \tag{41}$$

Taking the length scale close to the wall as proportional to y, using $l = k^{1/2}/\varepsilon$ and equation (41), one has,

$$\varepsilon = U^{*3}/\kappa y. \tag{42}$$

For the fully turbulent region in question, molecular heat transport may be significant for the case of liquid metals. It is assumed that the temperature profile between wall and the junction point is linear, or,

$$T^+ = y^+ Pr \tag{43}$$

where

$$T^+ = \frac{T_w - T}{T^*}, \quad T^* = q_w/\rho c_p U^*;$$

T = temperature at the junction point,

T_w = temperature at the wall.

For the g equation, the present experiments in the near wall region ($y^+ < 100$) were correlated in terms of the nondimensional temperature variance, $\sqrt{2g}/T^*$. The results can be expressed as,

$$\frac{\sqrt{2g}}{T^*} = y^+ Re^{0.0258} + 0.87 \times 10^{-5} Re. \tag{44}$$

Equation (44) indicates that the scalar scale is linear with y^+ from the wall to the region of validity of (40), and it is used as a 'wall function' for g in the near wall region.

CONSTANTS AND SUMMARY OF EQUATIONS

The three constants introduced, namely $c_{j\theta}$, c_g, and σ_g are here determined. All the other constants are taken from ref. [12] and will just be given.

To bring the level of calculated $\overline{u\theta}$, $\overline{v\theta}$ and g to the same level of measurements of Flaherty [10], Hochreiter [9] and present measurements, the constants $c_{j\theta}$ and c_g were taken as 0.004. It should be mentioned that the uncertainty and scatter of turbulent measurements in liquid metals do not allow a confident assignment of values to those constants. As more data are gathered, the degree of uncertainty can be reduced. Nevertheless, the use of the above constants is here assumed as a first approximation in the absence of better information. A sensitivity analysis using different values of $c_{j\theta}$ and c_g is shown in [28].

The constant σ_g takes the value of 0.72 so that when $Pr = 1$ and R approaches $R_\infty = 0.8$, the overall turbulent coefficient for g takes the value $\mu_t/0.9$, which is the same used by Spalding [30] and Plumb and Kennedy [31].

A summary of the equations written in their thin

Table 1. Model equations and constants

Var.	Conv.	Diffusion	Source/sink: Mean flow production	Buoyancy production	Viscous destruction	Pressure–strain scrambling: Non-buoyant contribution	Pressure–strain scrambling: Buoyant contribution
U	$\frac{DU}{Dt}$	$\frac{\partial}{\partial y}\nu_t\frac{\partial u}{\partial y}$	$-\frac{1}{\rho}\frac{dP}{dx}$	g_x			
T	$\frac{DT}{Dt}$	$\frac{\partial}{\partial y}\left(\frac{\nu}{Pr}+\frac{\nu_t}{\sigma_t}\right)\frac{\partial T}{\partial y}$					
k	$\frac{Dk}{Dt}$	$\frac{\partial}{\partial y}\left(\frac{\nu_t}{\sigma_k}\right)\frac{\partial k}{\partial y}$	$-\overline{uv}\frac{\partial U}{\partial y}=P$	$\frac{\beta}{T}g_x\overline{u\theta}=G$	$-\varepsilon$		
ε	$\frac{D\varepsilon}{Dt}$	$\frac{\partial}{\partial y}\left(\frac{\nu_t}{\sigma_\varepsilon}\right)\frac{\partial \varepsilon}{\partial y}$	$-c_{\varepsilon 1}\frac{\varepsilon}{k}\overline{uv}\frac{\partial U}{\partial y}$	$c_{\varepsilon 3}\frac{\varepsilon}{k}\frac{\beta}{T}g_x\overline{u\theta}$	$-c_{\varepsilon 2}\frac{\varepsilon^2}{k}$		
g	$\frac{Dg}{Dt}$	$\frac{\partial}{\partial y}\left(\frac{\nu}{Pr}+\frac{\nu_t}{\sigma_\theta}\right)\frac{\partial g}{\partial y}$	$-\overline{v\theta}\frac{\partial T}{\partial y}$		$-\frac{g\varepsilon}{kR}$		
$\overline{u\theta}$	$\frac{D\overline{u\theta}}{Dt}$	Diff. $\overline{u\theta}$	$-\overline{uv}\frac{\partial T}{\partial y}-\overline{v\theta}\frac{\partial U}{\partial y}$	$2\frac{\beta}{T}g_x g$		$-c_{1\theta}\frac{\varepsilon}{k}\overline{u\theta}F_1(Pe_t)+c_{2\theta}\overline{v\theta}\frac{\partial U}{\partial y}$	$-c_{3\theta}\frac{\beta}{T}g_x 2g$
$\overline{v\theta}$	$\frac{D\overline{v\theta}}{Dt}$	Diff. $\overline{v\theta}$	$-\overline{v^2}\frac{\partial T}{\partial y}$			$-\frac{\varepsilon}{k}F_1(Pe_t)[c_{1\theta}+c'_{1\theta}f]\overline{v\theta}$	
$\overline{uv}$	$\frac{D\overline{vu}}{Dt}$	Diff. $\overline{uv}$	$-\overline{v^2}\frac{\partial U}{\partial y}$	$\frac{\beta}{T}g_x\overline{v\theta}$		$-c_1\frac{\varepsilon}{k}\overline{uv}\left(1+\frac{3}{2}\frac{c'_1}{c_1}f\right)$ $+c_2\left(1-\frac{3}{2}c'_2 f\right)\overline{v^2}\frac{\partial U}{\partial y}$	$-c_3\frac{\beta}{T}g_x\overline{v\theta}$
$\overline{v^2}$	$\frac{D\overline{v^2}}{Dt}$	Diff. $\overline{v^2}$			$-\frac{2}{3}\varepsilon$	$-c_1\frac{\varepsilon}{k}\left[\left(1+2\frac{c'_1}{c_1}f\right)\overline{v^2}-\frac{2}{3}k\right]$ $-\frac{2}{3}c_2(1-2c'_2 f)\overline{uv}\frac{\partial U}{\partial y}$	

Constants in the turbulence model

$c_{\varepsilon 1}$	$c_{\varepsilon 2}$	$c_{\varepsilon 3}$	σ_k	σ_ε	c_1	c_2	c_3	c_w	c'_1	c'_2	$c_{1\theta}$	$c_{2\theta}$	$c_{3\theta}$	$c'_{1\theta}$	σ_g
1.44	1.92	1.44	1.0	1.3	1.8	0.6	0.6	3.72	0.6	0.3	3.0	0.5	0.5	0.5	0.72

shear layer form, as applicable to pipe flow analysis, is shown in Table 1. Also shown are model constants.

COMPUTATIONAL DETAILS

A finite difference solution scheme was applied to the set of equations for thin shear layers presented above. The calculations were performed for hydrodynamic developed pipe flow with uniform wall heat flux.

The computer program modified to include the turbulence model is an early version of the Patankar and Spalding [29] code called STAN5. In the original program, turbulence was calculated with only 'zero' and 'one-equation' models, in a fully explicit manner. To overcome possible numerical instabilities resulting from the more sophisticated representation developed here, a new treatment for the sources terms in the turbulence equations was devised with some basic reprogramming required to adopt it.

The geometry simulated corresponds to the heat transfer facility at the Nuclear Engineering Laboratories at Purdue University. An adiabatic entry length of 65 diameters was used before a heated length of another 67 diameters. This total of 132 diameters required an average of 280 integrations in the streamwise direction.

RESULTS AND DISCUSSION

Isothermal results

Although this work was primarily concerned with nonisothermal flow, calculations were also performed for isothermal flow, in the range of $30\,000 < Re < 90\,000$, to provide a reference and check the model performance by predicting unheated flow in the Reynolds range of interest for the heated measurements.

Figure 2 shows results for the mean velocity as compared with experiments of Eyler [22]. Agreement seems reasonable except near the centerline. In this work, all mean velocity profiles are underpredicted at the centerline. This is a result of the inability of the model to represent the turbulent velocity length scale decreasing in the near centerline region. This point will be discussed later. Here it will suffice to say that a larger length scale at the centerline causes a larger coefficient of momentum exchange, μ_t, and therefore a flatter profile at the center.

Figures 3 and 4 compare predictions for k and ε with Laufer's measurement in air [32]. It is seen that the calculated values at $y/R < 0.3$ for k are slightly larger than the experimental data. That is in agreement with what was said previously about the turbulent coefficient of exchange, $\mu_t = \rho c_\mu k^2/\varepsilon$, since larger values for k imply larger values for μ_t and then a flatter velocity profile.

The nondimensional turbulent shear stress is shown in Fig. 5, compared with Hochreiter's results for mercury [9] and Laufer's data for air [32]. Agreement seems good over most of the flow cross section. The reason for the sudden increase in the predictions in the wall region is two-fold. First, the equation describing $\overline{uv}$, equation (32), is written with the local equilibrium approximation, or (Conv. − Diff.) = 0. Close to the wall, this is not expected to hold, since diffusion transport in the cross stream direction may be of some significance. Second, the evaluation of velocity derivatives close to the wall is dependent on the grid mesh used, and so production terms in the $\overline{uv}$ equations are sensitive to grid point distribution. Because of reason (a), the absence of a diffusive term on the $\overline{uv}$ equations *does not* 'smooth' the differences out. This can be seen by referring to results for k and ε, Figs. 3 and 4, where no 'kinks' are present. In addition, extensive testing using several grid spacings in the wall region has shown the dependent variables U, k and ε to be much less sensitive to the wall grid distribution than $\overline{uv}$ itself. For that reason, nonisothermal results to be shown later were calculated with a more inexpensive coarse grid near the wall.

Figure 6 compares predicted values for the lateral velocity fluctuations component $\sqrt{\overline{v^2}}/U^*$ with Hochreiter and Laufer results. The wall damping effect, showed more clearly by Laufer's results, is obtained for distances very close to the wall. This may be an indication for a need for a more elaborate wall correction for the pressure strain correlation. In this work, use was made of a simple wall correction presented by Ljuboja and Rodi for wall-jets [12].

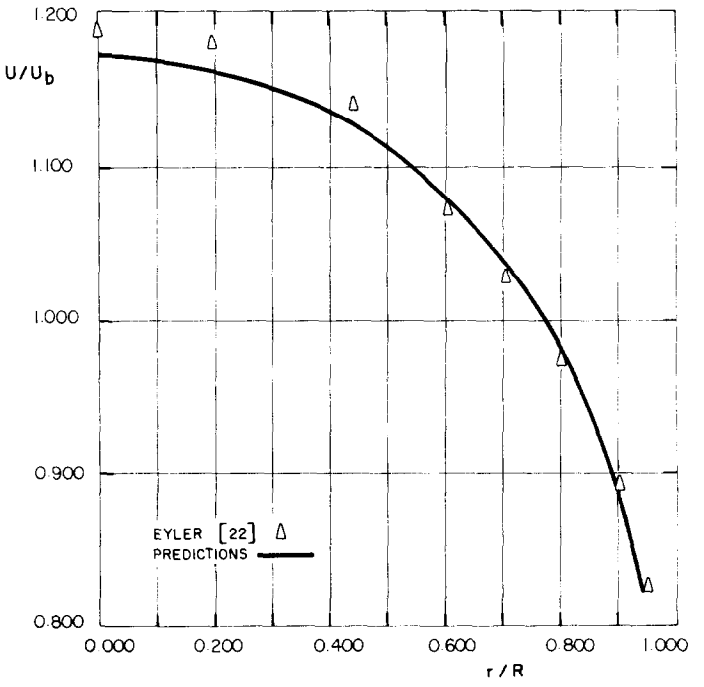

FIG. 2. Comparison of measured and predicted isothermal mean velocity, U, $Re = 50{,}000$.

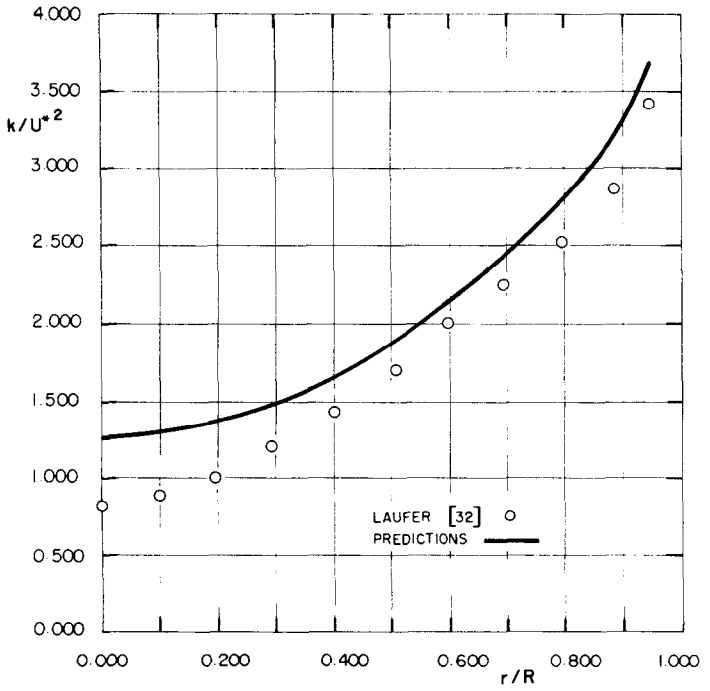

FIG. 3. Comparison of measured and predicted isothermal kinetic energy, k, $Re = 50{,}000$.

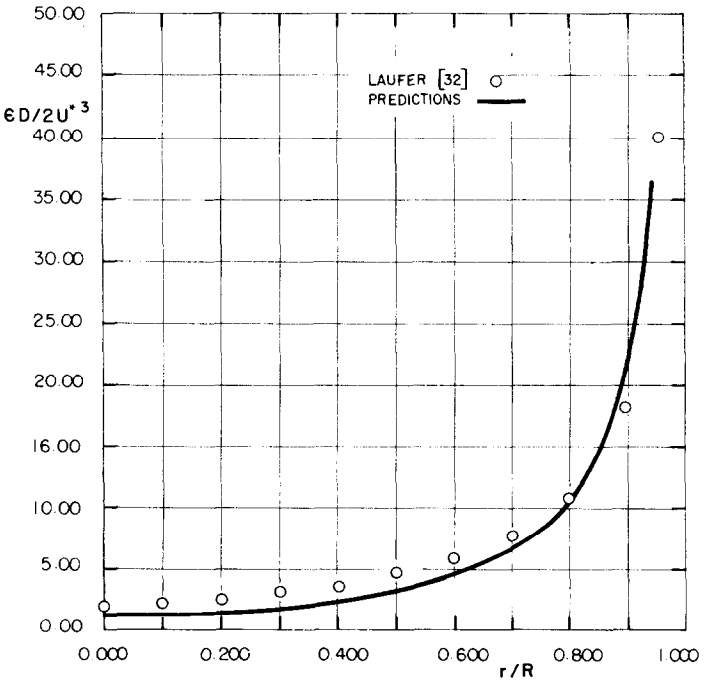

FIG. 4. Comparison of measured and predicted isothermal dissipation rate of turbulent kinetic energy, ε, $Re = 50{,}000$.

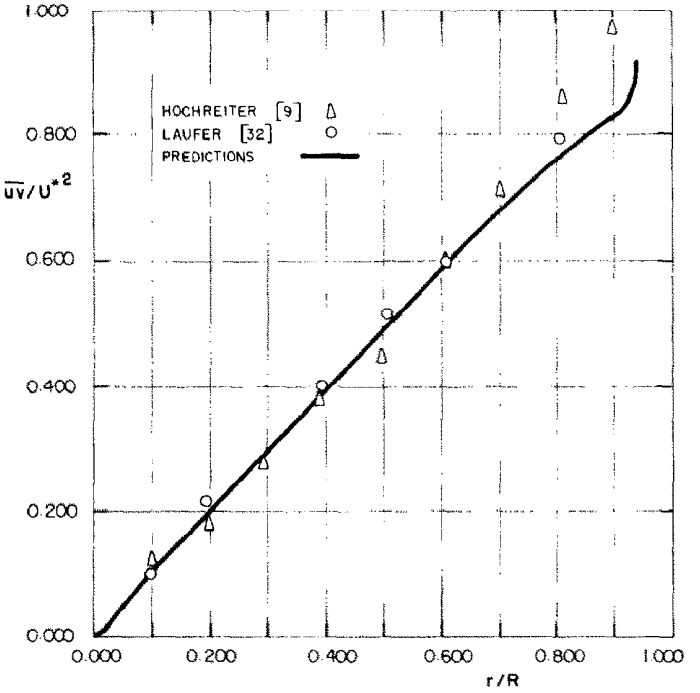

FIG. 5. Comparison of measured and predicted isothermal lateral turbulent shear stress, $\overline{uv}$, $Re = 50{,}000$.

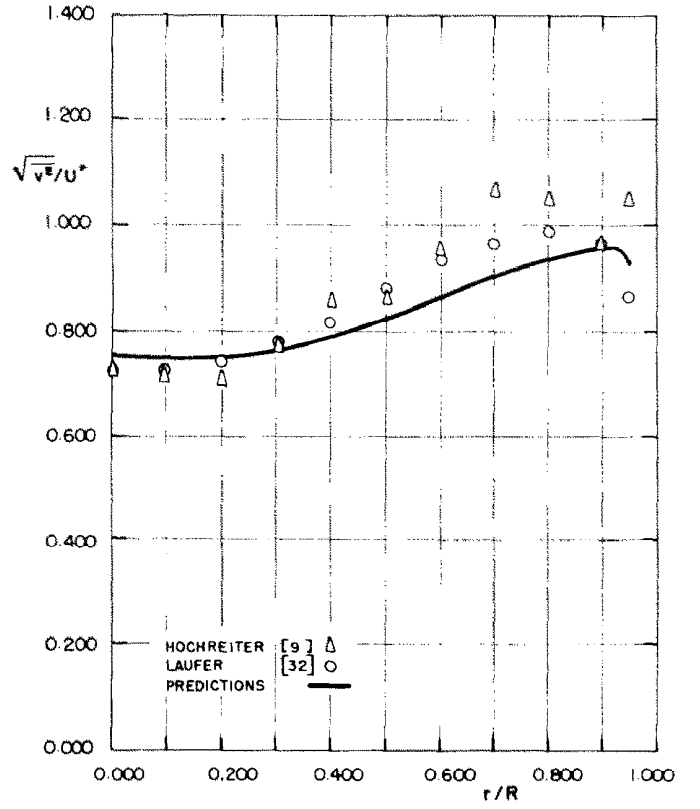

FIG. 6. Comparison of measured and predicted isothermal lateral velocity fluctuation, $\overline{v^2}$, $Re = 50{,}000$.

Table 2. Comparison of predicted friction factor with Blasius formula for isothermal flow

Re	f calculated	$f = 0.079Re^{-0.25}$	% error
18471	0.00662	0.00678	−2.3
29851	0.00598	0.00601	−0.5
46694	0.00542	0.00537	+0.9
56057	0.00520	0.00513	+1.3
89359	0.00480	0.00457	+5.0

Launder and Samaraweera [33] used a more complicated version of the wall correction for calculating confined flows, but no results on $\sqrt{\overline{v^2}}/U^*$ for pipes were presented. Therefore, an assessment on π_{ij} wall corrections is still limited by lack of testing in the literature.

Friction factors, f, were calculated and compared with Blasius formula, $f = 0.079\ Re^{-0.25}$. Results are shown in Table 2. The errors of the predictions are within +5% in relation to the Blasius smooth pipe formula.

Nonisothermal results

This section presents results for mean and turbulent quantities as functions of the buoyancy parameter Ra/Re^2, where

$$Ra = Gr_A\ Re = \text{Rayleigh number},$$

$Gr_A = \rho^2\beta g A D^4/\mu^2$ = Grashof number based on A, and $A = dT/dx$ is axial temperature gradient. In this work, the parameter Ra/Re^2 is used as a buoyancy factor as suggested by Bird *et al.* [34].

The hydrodynamic field

Figures 7 and 8 show comparisons of predictions with experiments of Jacoby [5] for $30\,000 < Re < 60\,000$. The results qualitatively describe the distortion on the mean flow. However, in most of the Ra/Re^2 covered, the amount of distortion is underpredicted. The reason for these discrepancies can be explained as partially due to modeling and partially due to the numerics used. First, in Figs. 7 and 8 the flatter calculated profiles for U near the centerline may be due to the relatively large calculated length scale in this region, in a manner similar to what was said for isothermal flow. The second reason has its grounds in the numerical aspect.

Although the treatment of the source terms was changed from the original PS method to avoid possible numerical instabilities, the explicit handling of the effective diffusion coefficients was kept the same. This was done to keep linear the set of algebraic equations obtained from discretizing the balance equations. This fact enables the use of a direct, noniterative numerical algorithm for solution of the algebraic relations. However, for high heat rate cases, fluid properties variation along the axial direction of integration implies a nonlinear set of equations, in the sense that the finite difference coefficients have then to be updated by successive iterations in each forward step. Although the use of a nondirect, iterative numerical method seems to

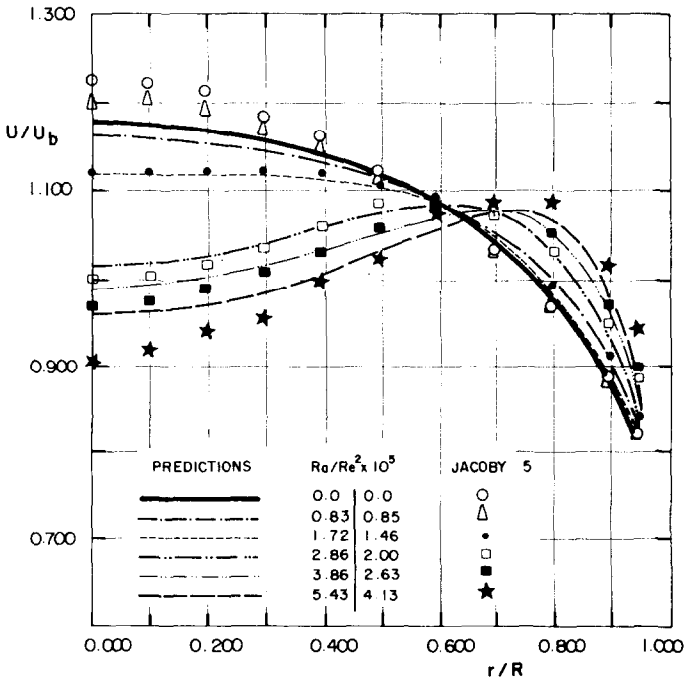

FIG. 7. Comparison of measured and predicted mean velocity, U, Re = 30,000.

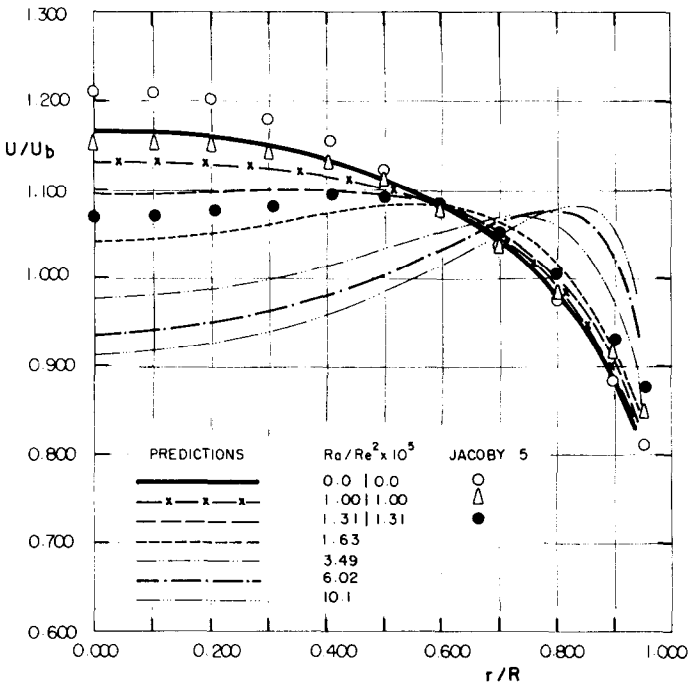

FIG. 8. Effect of heating on mean velocity, U, $Re = 60{,}000$.

be suitable for solving cases with high wall heat loads, in this work a direct solution technique, known in the literature as the Tri-Diagonal Matrix Algorithm (TDMA) was used. The justification for using the TDMA scheme lies in the fact that the accuracy obtained by using an iterative solution procedure would not be consistent with accompanying uncertainties of several proposed model relations as well as discrepancies associated with experimental liquid metal data. The absence of an iterative procedure to correct for properties variation along the streamwise flow direction caused an error of about 15% when the total heat input through the wall was compared to the heat carried by the fluid. This cumulative error was referent to the highest buoyancy parameter used ($Ra/Re^2 = 2.99 \times 10^{-4}$) and to approx. 280 forward steps.

For the reasons stated above, including uncertainty in the quantitative aspect of the model predictions and inherent difficulties associated with the numerics used, in this work one tried to investigate only the *qualitative* aspect of changes in the variables as a function of the buoyancy parameter, Ra/Re^2.

Figure 9 presents the effect of heating in the turbulent kinetic energy. The initial damping and posterior enhancement of turbulent exchange, as claimed by Petukov's papers [1, 35] is qualitatively predicted.

Figure 10 presents results for the turbulent shear stress, $\overline{uv}$. The kinks near the wall are the result of the use of a less expensive grid spacing close to the wall. As mentioned for the results for isothermal cases, this is due to the absence of a diffusion term in the $\overline{uv}$ equation that physically smooths out differences in calcuating velocity derivatives in the near wall region. The use of a coarse grid, however, did not cause detectable differences for variables described by a transport equation, namely U, T, k, ε and g.

Figure 11 shows the behavior for $\sqrt{\overline{v^2}}/U^*$ similar to the one for k. This figure suggests that gravity also has an influence on the turbulent structure in the directions perpendicular to the gravity field. This is in agreement with the review of Launder [19], and shows the connection among turbulent stresses in a gravity affected field. Although no direct influence exists of gravity on $\overline{v^2}$, the dependence of $\overline{v^2}$ on stresses aligned in the axial direction causes an indirect affect on it. This is seen by inspecting the existing interlinkage among the stresses, represented in Table 1.

The ratio of lateral to total kinetic energy is shown in Fig. 12. The figure shows a substantial difference of heated $\overline{v^2}/k$ predictions when compared with the unheated profile, which is monotonously decreasing to the wall. A 'peak' appears in the core region and approaches the wall as Ra/Re^2 increases. The figure suggests that although k and $\overline{v^2}$ are damped by buoyancy in the near wall region, the lateral fluctuations are less sensitive to these changes than the axial velocity fluctuations, $\overline{u^2}$, which is aligned with the gravity vector and so directly influenced by gravity. Thus, in this region, lateral fluctuations will carry relatively more energy when buoyancy is present than in the isothermal case. In this work, no equation is used

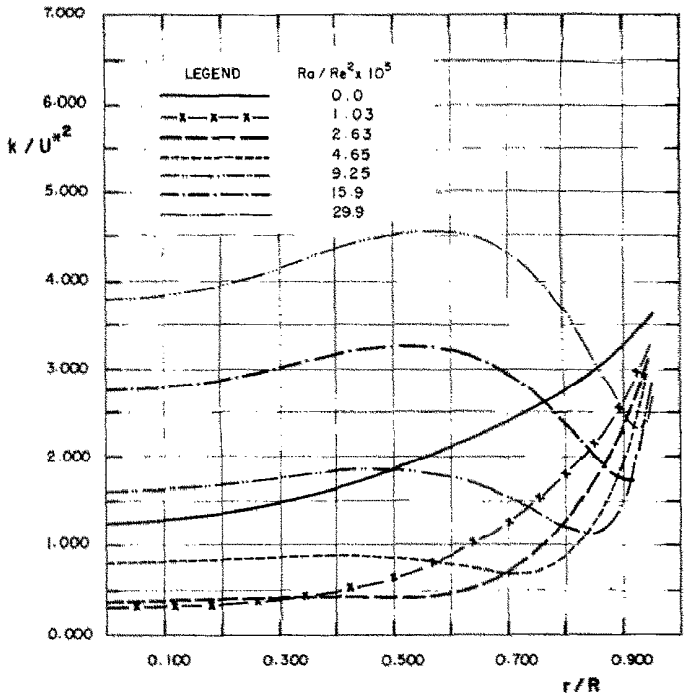

FIG. 9. Effect of heating on turbulent kinetic energy, k, $Re = 30{,}000$.

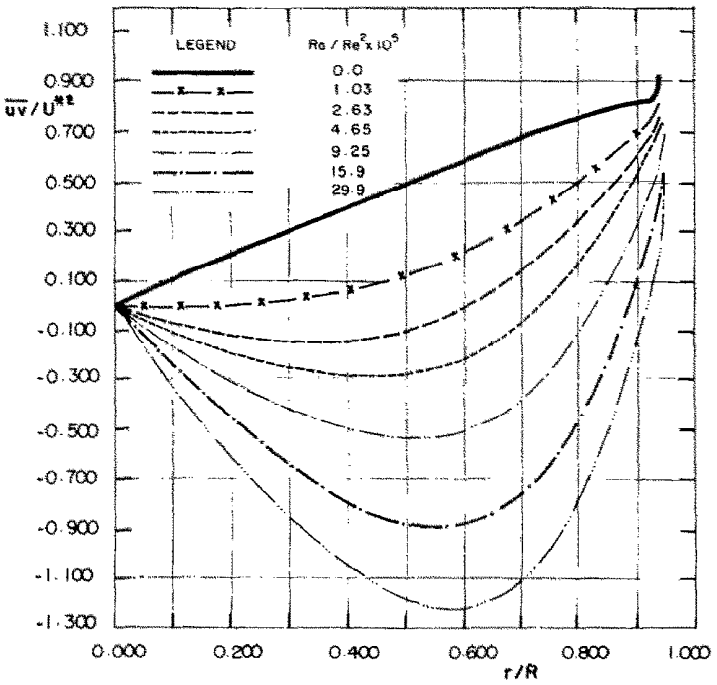

FIG. 10. Effect of heating on lateral turbulent shear stress, $\overline{uv}$, $Re = 30{,}000$.

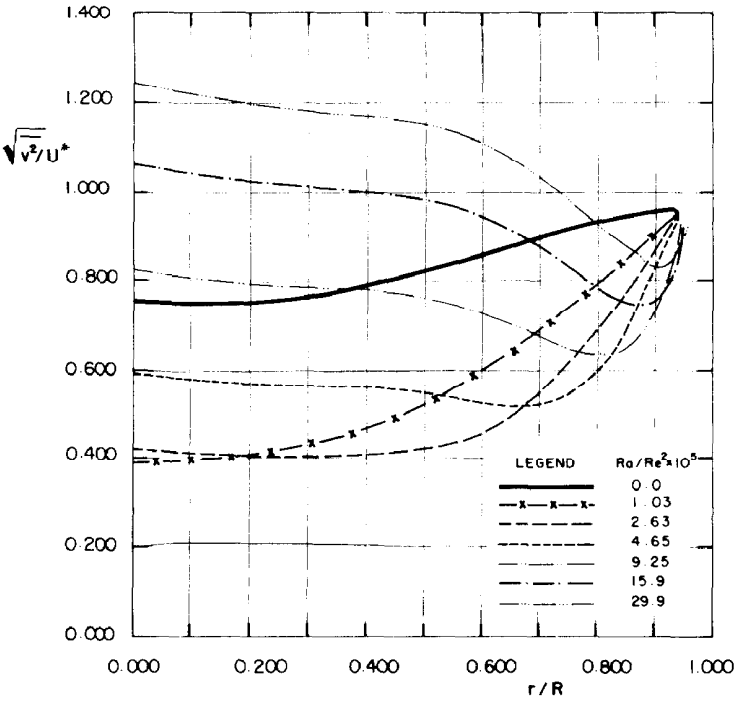

FIG. 11. Effect of heating on lateral velocity fluctuations, $\overline{v^2}$, $Re = 30{,}000$.

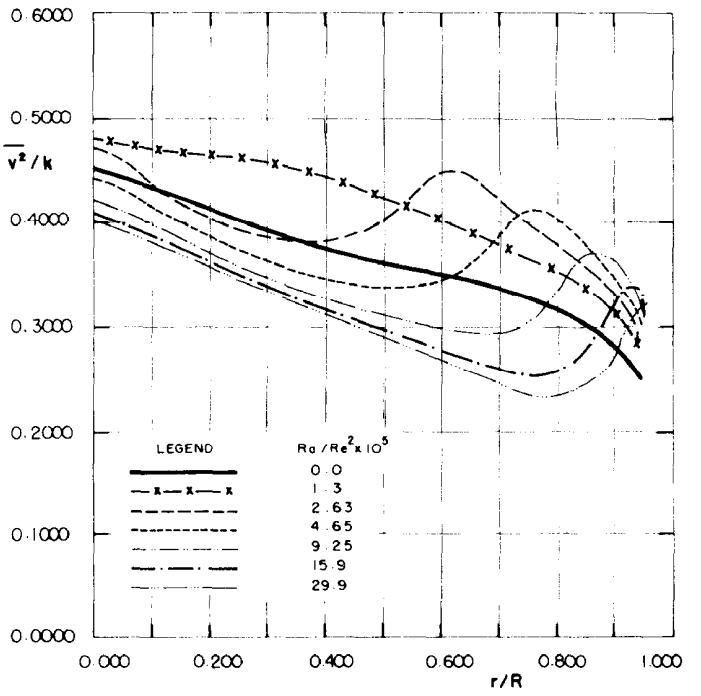

FIG. 12. Effect of heating on the ratio of lateral to total turbulent kinetic energy $\overline{v^2}/k$, $Re = 30{,}000$.

to describe the axial velocity fluctuation and an assessment on the effects of buoyancy on it can only be roughly pictured.

The thermal field

Temperature profiles are shown in Fig. 13. Results are compared with experiments of Jacoby [5]. The predictions qualitatively follow the experimental trends. An initial tendency towards a radial linear dependence followed by a flattening of the temperature profile is well calculated. The first stage represents a decrease in turbulent exchange and the second one an enhancement in the lateral turbulent transport. Those trends are in agreement with Petukhov's explanation for the initial decrease and posterior increase in Nu, as a function of wall heating. Calculated Nus are presented later.

In order to bring the level of calculated radial heat fluxes to a level on the order of existing experiments, the constant $c_{j\theta}$ in equation (20) was set as 0.004. This constant comes from the modeling of the dissipation process, $\varepsilon_{j\theta}$, which physically can be seen as a sink for the heat flux, $\overline{u_j\theta}$. Thus, the introduced constant, $c_{j\theta}$, primarily controls the level of $\overline{u_j\theta}$.

Figure 14 compares calculated and measured radial turbulent heat fluxes for mercury at $Re = 50{,}000$. These measurements constitute a pioneering effort at Purdue University during the 1970s in picturing turbulence structure in nonisothermal liquid metal flow [9, 10, 36]. The figure reflects the degree of difficulty in obtaining reliable experimental information on this quantity, and the scatter and uncertainty in the data limit the degree of confidence in assigning a numerical value to $c_{j\theta}$. The value here used should be considered as a first approximation subjected to refinement as more data are gathered.

Figure 15 shows calculated radial turbulent heat fluxes. The predictions show that an initial decrease in the level of $\overline{v\theta}$ precedes a posterior increase, as the Ra/Re^2 increases. This idea is also in agreement with the predictions shown so far. The figure shows some irregularities in the calculated profiles near the wall for relatively large wall heat fluxes. At the stage of this research, the lack of explanation for those irregularities has its grounds in the difficulty to identify whether a numerical or a modeling inconsistency exists which causes the aforementioned anomalies.

A compilation of axial turbulent heat flux measurements for various Pr is shown in Fig. 16 [8, 9, 10, 23, 24, 37]. (The figure is plotted for $-\overline{u\theta}/U^*T^*$, showing the opposite direction for the fluxes for a system oriented upward). The results for air of Carr *et al.* [8] and for mercury by Hochreiter [9] and Flaherty [10] obtained at high wall heat loads show a reversal in direction of the axial heat flux. This trend is more easily seen with the Carr *et al.* experiments for two increasing

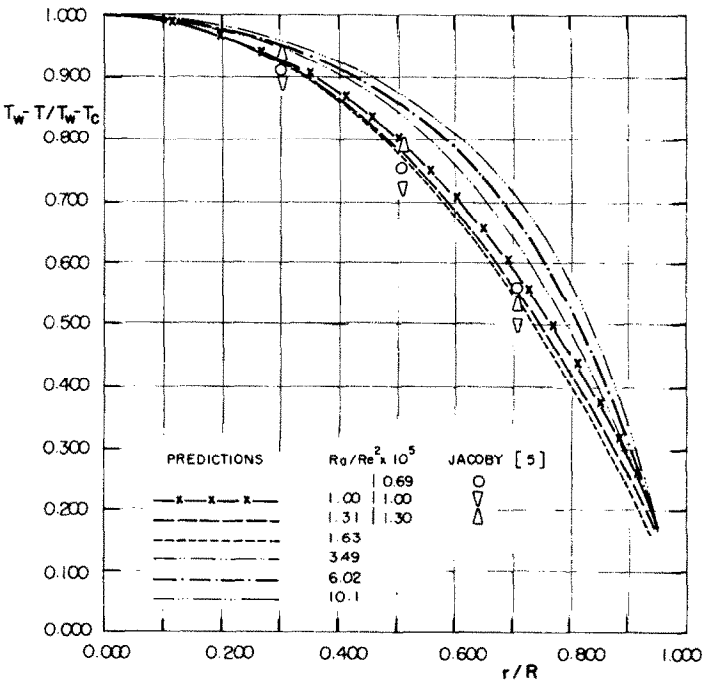

FIG. 13. Comparison of measured and predicted mean temperature, T, $Re = 60{,}000$.

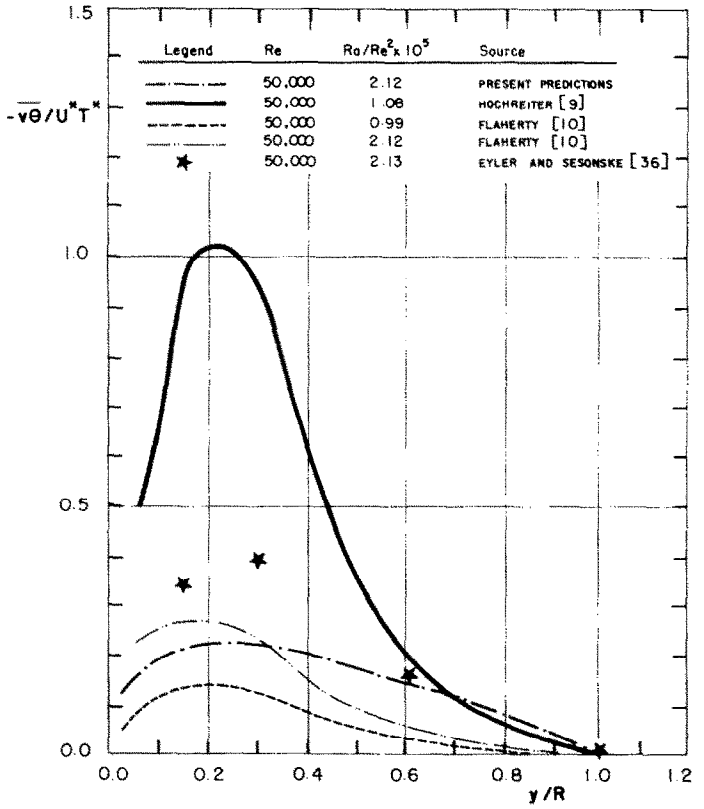

FIG. 14. Comparison of measured and predicted radial turbulent heat flux, $\overline{v\theta}$, $Re = 50{,}000$.

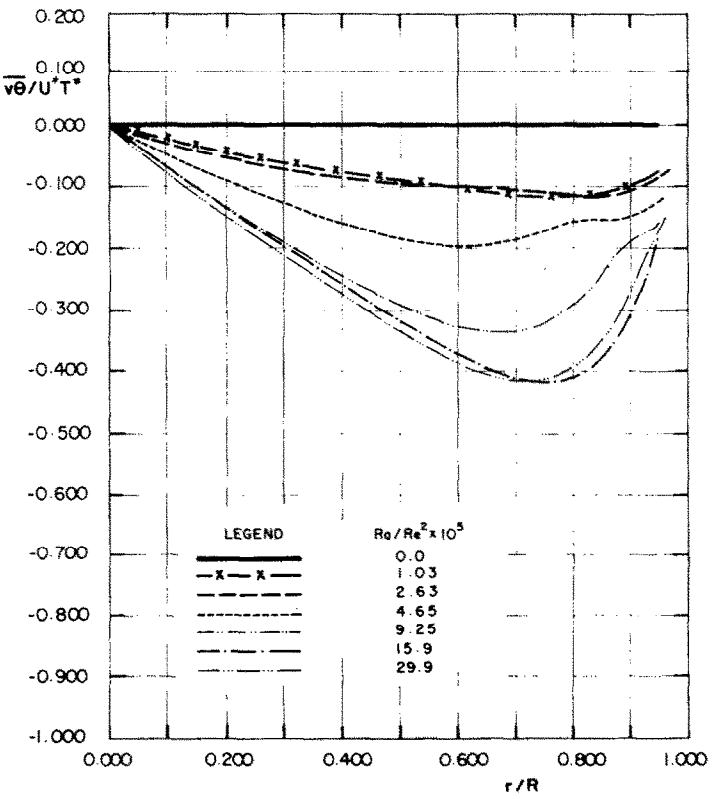

FIG. 15. Effect of heating on radial turbulent heat flux, $\overline{v\theta}$, $Re = 30{,}000$.

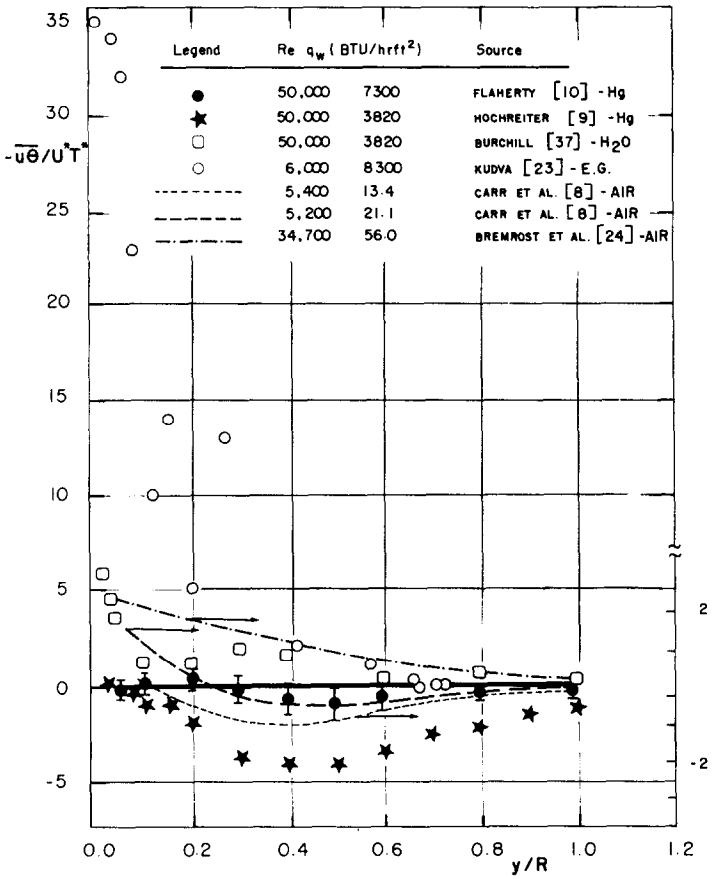

FIG. 16. Measured axial heat flux in air, water, mercury and ethylene glycol.

wall heat fluxes. The model used in the present work predicts the axial turbulent heat flux behavior, as the buoyancy parameters Ra/Re^2 increases.

Figure 17 presents results for $\overline{u\theta}$. The predictions show a reversal and continuous increasing of the magnitude of $\overline{u\theta}$. The onset of reversal, as well as quantitative comparison with experiments, are of difficult analysis due to already mentioned uncertainties in the experiments and on the modeling proposals. The calculated values for the same experimental conditions are roughly one-fourth of Flaherty's data.

Temperature fluctuations were measured for $Re = 30{,}000$, $Re = 60{,}000$ and four wall heat fluxes. Figure 18 shows a comparison of measured temperature fluctuations for mercury with the present measurements [9, 22, 38]. The present results agree with Hochreiter's [9], and Loos's [38] data, but are slightly larger than Eyler's [22] measurements. Eyler used a different hot film calibration procedure than Hochreiter and Loos. Although the probe calibration used in this work is different from Hochreiter's and Eyler's, it is more similar to the Hochreiter work.

Another source for the differences among data is the counting time for obtaining the r.m.s. of the signal and system noise. Caruso [39], whose data is in agreement with Eyler's, reported a waiting time on the order of 3.6 time constants (360s). Since in liquid metals most of the information on the turbulent temperature fluctuations are at relatively low frequencies, in this work a period of five time constants was used to assure that fluctuations on the low cycle part of the spectrum were counted. In doing this, however, a relatively high value for the r.m.s. was obtained, possibly due to counting of 60 cycle noise from the electrical heaters. A study on the low cycle noise in liquid metals is reported by Hochreiter [40]. Preliminary data analysis found the present results to be on the average of 15% higher than the Hochreiter and Loos data, and since differences in the calibration use by them and the present work did not amount to more than a few percent, the present data were corrected in 15% to a level compatible with Hochreiter and Loos data. This procedure was found to be a good approximation, since a quantitative analysis of existing electrical noise in the system is difficult to access. In addition, this correction was done for all data, and relative trends among measurements were kept the same.

Fig. 19 shows measured and calculated results for $g = \overline{\theta^2}/2$. The introduced constant, c_g, was taken as

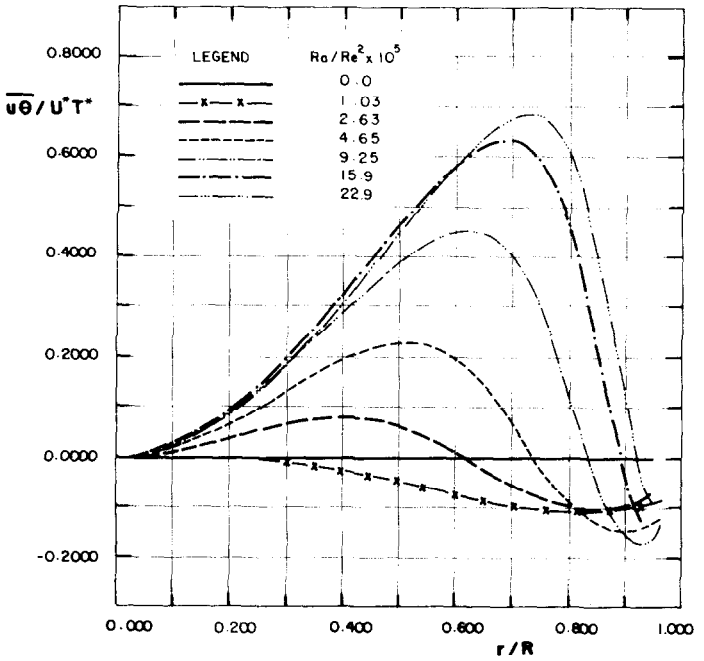

FIG. 17. Effect of heating on axial turbulent heat flux, $\overline{u\theta}$, $Re = 30{,}000$.

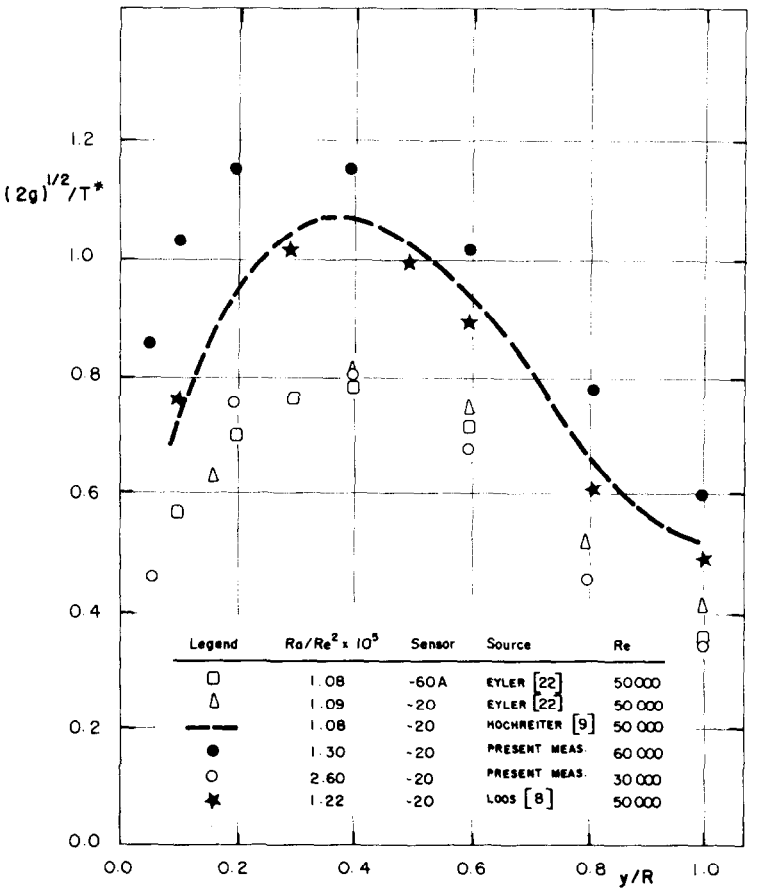

FIG. 18. Comparison of measured temperature fluctuations in mercury.

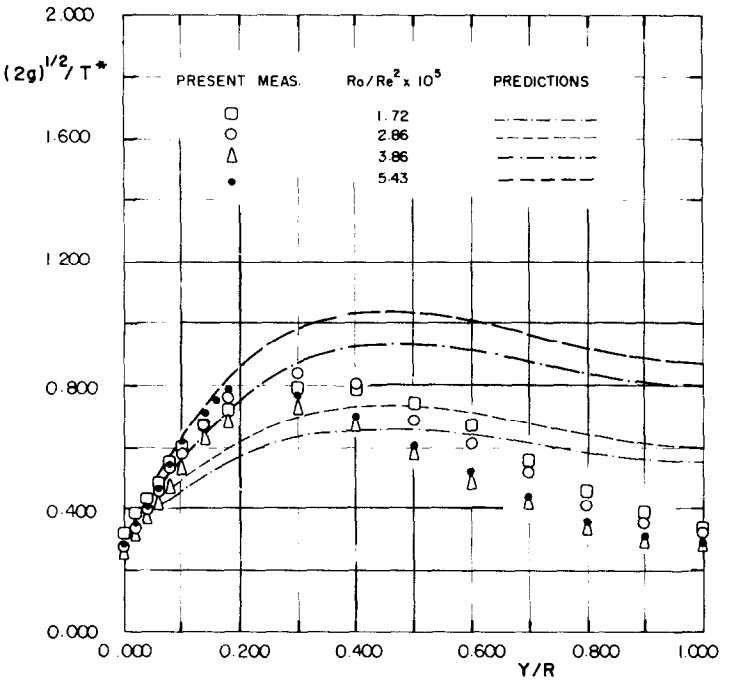

FIG. 19. Comparison of measured and calculated temperature fluctuations, $Re = 30{,}000$.

0.004 to give best agreement near the wall. In Fig. 19, the centerline region is substantially overpredicted. Yet, the calculations showed an increase in $\sqrt{\overline{\theta^2}/T^*}$ as Ra/Re^2 increases, while the experiments showed a decrease within the same range. In this work, an attempt was made to model the g equation to correctly follow the dependence on Ra/Re^2, but it is recognized that further work is needed to approximate all the terms in the equation. Extensive numerical work was performed showing that even by totally eliminating the turbulent diffusion in the diffusive term of g, the centerline region was still overpredicted. This may be an indication that the productive term, P_g, and the dissipative term, ε_g, need further refinement, especially near the centerline. In order to accomplish reliable modeling for the particular case of the g equation in a

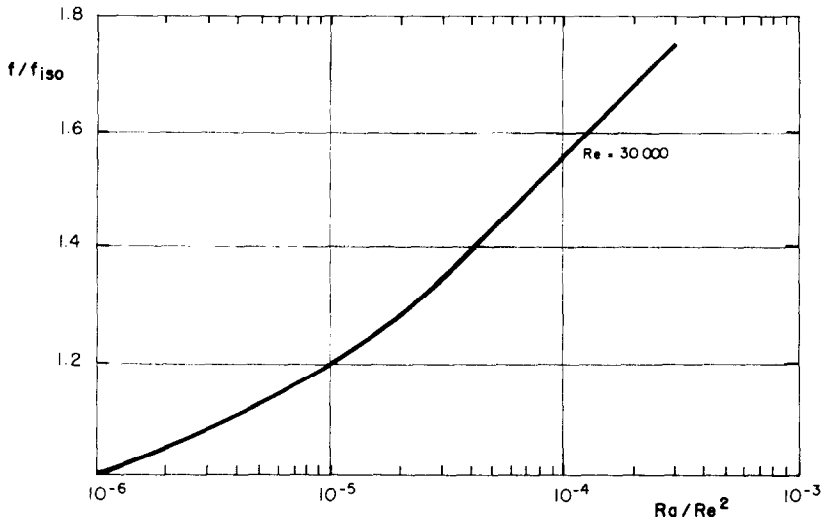

FIG. 20. Calculated relative Fanning friction factor, f/f_{iso}.

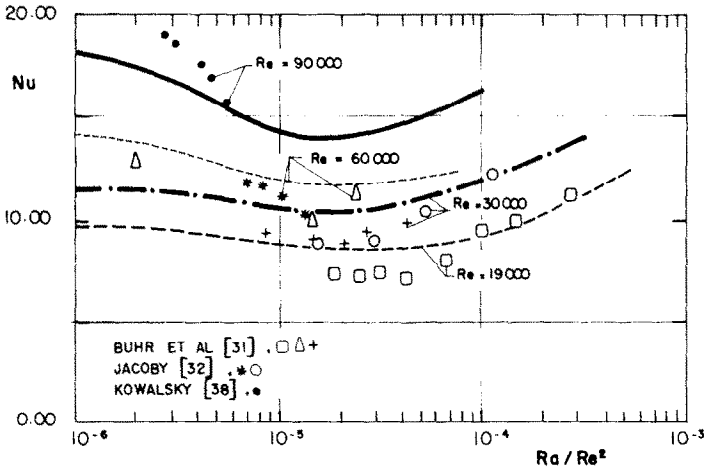

FIG. 21. Comparison of measured and calculated Nusselt number.

more systematic way, this research identifies the necessity of experimental programs for measuring individual terms in the g equation for the flow under consideration. After more understanding of the process which individually accounts for the total level of g, uncertainties occurring in modeling it can be reduced.

Friction factor and Nusselt number

Figure 20 shows the calculated skin friction factor, f, for increasing Ra/Re^2. The results are normalized by the isothermal friction factor, f_{iso}, obtained for very small heat loads. The increase in f is due to the increasing of the velocity derivative at the wall, which is presented in Figs. 7, 8. The results are in qualitative agreement with the measurements in water presented in Petukhov's review paper [35]. The calculated Nusselt number is compared in Fig. 21 with measurements of Jacoby [5], Kowalski [6], and Buhr [41] for mercury. The figure compares *absolute* values and shows the initial decrease in Nu due to damping in turbulent transfer, as claimed by Petukhov [35]. In addition, the calculations suggest that the higher the Reynolds number, the higher the amount of damping. This fact is also shown by Polyakov [41], who presented a theoretical analysis for the boundaries of influence of free convection in pipe flow of mercury.

CONCLUSIONS AND RECOMMENDATIONS

This research was primarily concerned with the development of a predictive technique able to calculate the influence of buoyancy in a vertical flow of mercury in a pipe. Test calculations for isothermal flow showed good performance in predicting turbulent and mean flows.

Further results showed that distortion occurring in the nonisothermal time-averaged flow is qualitatively predicted. Calculation for the skin friction factor and Nu are also in qualitative agreement with the literature.

The turbulent field is shown to be affected by buoyancy, although a more accurate assessment on the performance of the model here used is limited by the lack of experimentation under this situation. The initial damping and posterior enhancement of turbulent transfer as Ra/Re^2 increases is well predicted and shown in results for k, $\overline{v^2}$ and $\overline{v\theta}$. The reversal of $\overline{u\theta}$ under the influence of buoyancy, also presented in several experiments, is shown to be calculable by the present model.

Results for temperature fluctuations are regarded as a first approximation, requiring further work.

As recommendations, this research identifies the need for more data on the turbulence structure for the particular case of buoyancy affected flow, although it is recognized that existing data in nonbuoyancy flows are scarce and subjected to experimental uncertainties. This is particularly true for heated mercury flow measurements where available experimental techniques require extreme care for obtaining reliable data.

Major experimental programs for measuring the turbulent correlation $\overline{v\theta}$ and $\overline{u\theta}$ are found to be needed for improving modeling assumptions. In the particular case of the g equation, measurements of the individual terms in the equation can provide insight for a more reliable modeled form to represent the different processes of diffusion, production and dissipation. In the recent review of Launder [19], this state of affairs was also suggested, particularly on referring to the dissipation term, ε_g. Launder mentions that a two-prong thermocouple probe is able to measure ε_g, whereas a direct measure of the dissipation of turbulent kinetic energy, ε, is known to be of more difficulty.

Acknowledgements—The first author wishes to thank CNEN-Comissão Nacional de Energia Nuclear and CNPq-Conselho Nacional de Desenvolvimento Científico e Tecnológico, Brazil, for their financial support during the preparation of this work. The suggestions of Dr. L. L. Eyler are gratefully appreciated.

REFERENCES

1. B. S. Petukhov, A. F. Polyakov and Yu. L. Shekhter, Turbulent flow and heat transfer in a gravitational field (Survey), *High Temp.* **16**, 531–547 (1978).
2. A. F. Polyakov, Turbulent forced flow in vertical channels under free convection conditions, *J. Engng Phys.* **35**, 801–811 (1978).
3. B. S. Petukhov and N. V. Metvetskaya, Turbulent flow and heat exchange in vertical pipes under conditions of strong influence of upward forces, *High Temp.* **17**, 665–672 (1979).
4. H. O. Buhr, E. A. Horsten and A. D. Carr, The distortion of turbulent and temperature profiles on heating for mercury in a vertical pipe, *J. Heat Transfer* **96**, 152–158 (1974).
5. J. K. Jacoby, Free convection distortion and eddy diffusivity effects in turbulent mercury heat transfer. M.S. thesis, Purdue University (1972).
6. D. K. Kowalski, Free convection distortion in turbulent mercury pipe flow. M.S. thesis, Purdue University (1974).
7. J. K. Jacoby and A. Sesonske, Free convection distortion and eddy diffusivity effects in turbulent mercury heat transfer, *Trans. Am. Nucl. Soc.* **15**, 408–409 (1972).
8. A. D. Carr, M. A. Connor and H. O. Buhr, Velocity temperature and turbulence measurements in air for pipe flow with combined free and forced convection, *J. Heat Transfer* **95**, 445–452 (1973).
9. L. E. Hochreiter and A. Sesonske, Turbulent structure of isothermal and non-isothermal liquid metal pipe flow, *Int. J. Heat Mass Transfer* **17**, 113–128 (1974).
10. T. W. Flaherty, An investigation of non-isothermal turbulent pipe flow of mercury. Ph.D. thesis, Purdue University (1974).
11. M. Ljubola and W. Rodi, Calculations of turbulent wall jets with an algebraic Reynolds stress model, *J. Heat Transfer* **102**, 350–356 (1980).
12. M. Ljuboja and W. Rodi, Prediction of horizontal and vertical turbulent buoyant wall jets, *J. Heat Transfer* **103**, 343–349 (1981).
13. B. E. Launder and D. B. Spalding, The numerical computation of turbulent flow, *Comp. Meth. Appl. Mech. Engng* **3**, 269–289 (1974).
14. B. E. Launder and D. B. Spalding, *Lectures in Mathematical Models of Turbulence*. Academic Press (1972).
15. W. T. Sha and B. E. Launder, A General Model for Turbulent Momentum and Heat Transport in Liquid Metals. DOE Report, ANL-77-78 (1979).
16. M. M. Gibson, Transport equations of turbulent flows. In Turbulence Models for Computational Fluid Dynamics, lecture notes, Penn State Univ. (1982).
17. J. L. Lumley, O. Zeman and J. Siess, The influence of buoyancy on turbulent transport, *J. Fluid Mech.* **84**, 581–597 (1978).
18. J. L. Lumley and B. Khajeh-Nouri, Computational modeling of turbulent transport, *Adv. Geophys.* **A18**, 169–192 (1974).
19. B. E. Launder, Heat and mass transport. In *Topics in Applied Physics*, Chap. 6, *Turbulence*, 2nd edn (Edited by P. Bradshaw). Springer, Berlin (1978).
20. K. Suzuki, An approach to liquid metal turbulent heat transfer in a circular tube solving $\overline{vt}$ equation with local equilibrium assumption, *Letters Heat Mass Transfer* **9**, 245–254 (1982).
21. H. Tennekes and J. L. Lumley, *A First Course in Turbulence*. MIT Press, Cambridge, Massachusetts (1972).
22. L. L. Eyler and A. Sesonske, Turbulent structure measurements in mercury pipe flow, *Int. J. Heat Mass Transfer* **23**, 1561–1572 (1980).
23. A. K. Kudva and A. Sesonske, Structure of turbulent velocity and temperature fields in ethylene glycol flow at low Reynolds numbers, *Int. J. Heat Mass Transfer* **15**, 127–145 (1972).
24. K. Bremhorst and K. J. Bullock, Spectral measurements of turbulent heat and momentum transport in fully developed pipe flow. *Int. J. Heat Mass Transfer* **13**, 2141–2154 (1973).
25. A. S. Monin, On symmetry properties of turbulence in the surface layer of air, *Atmos. Oceanic Phys.* **1**, 45 (1965).
26. P. L. Maksin, B. S. Petukhov and A. F. Polyakov, Balance of intensity of temperature pulsations in a turbulent flow of fluid, *High Temp.* **18**, 1028–1036 (1980).
27. W. Rodi, The prediction of free turbulent boundary layers by use of a two-equation model of turbulence. Ph.D. thesis, University of London, 1972.
28. M. J. S. de Lemos, Analytical and experimental study of combined free and forced convection in turbulent liquid metal pipe flow. Ph.D. thesis, Purdue University (1983).
29. S. V. Patankar and D. B. Spalding, *Heat and Mass Transfer in Boundary Layers*, 2nd edn. Intertext, London (1970).
30. D. B. Spalding, Concentration fluctuations in a round turbulent free jet, *Chem. Engng Sci.* **26**, 95–107 (1971).
31. O. A. Plumb and L. A. Kennedy, Application of the K–epsilon turbulence model to natural convection from a vertical isothermal surface. *J. Heat Transfer* **99**, 79–85 (1977).
32. J. Laufer, The structure of turbulence in fully developed pipe flow. Report, NACA-TR-1174, 1954.
33. B. E. Launder and D. S. A. Samaraweera, Application of a second-moment turbulence closure to heat and mass transport in their shear flows—I. Two-dimensional transport, *Int. J. Heat Mass Transfer* **22**, 1631–1643 (1979).
34. R. B. Bird, W. E. Stewart and E. N. Lightfoot, *Transport Phenomena*. John Wiley, New York (1960).
35. B. S. Petukhov, A. F. Polyakov and O. G. Martynenko, Buoyancy effect on heat transfer in forced channel flows. *Proc. Seventh International Heat Transfer Conference*, Paper RK5, Munich, ASME (1982).
36. L. L. Eyler and A. Sesonske, Turbulent heat fluxes in liquid–metal channel-flow models and experiments, *Trans. Am. Nucl. Soc.* **25**, 368–369 (1976).
37. W. E. Burchill, Statistical properties on velocity and temperature in isothermal and non-isothermal turbulent pipe flow. Ph.D. thesis, University of Illinois (1970).
38. R. L. Loos, Characteristics of turbulent temperature fluctuations in mercury. M.S. thesis, Purdue University (1971).
39. S. Caruso, Space–time correlations of temperature in turbulent mercury pipe flow. M.S. thesis, Purdue University (1977).
40. L. E. Hochreiter and A. Sesonske, Thermal turbulence characteristics in flowing sodium–potassium, *Int. J. Heat Mass Transfer* **12**, 114–118 (1969).
41. A. F. Polyakov, Limits and character of the start of thermogravitation effect on the turbulent flow and heat transfer of liquid metals in vertical tubes, *High Temp.* **15**, 676–681 (1977).

MODELISATION DE LA TURBULENCE DANS LA CONVECTION MIXTE PAR L'ECOULEMENT DE MERCURE DANS UN TUBE

Résumé—Un modèle simplifié algébrique des contraintes est utilisé pour étudier l'effet de la pesanteur sur l'écoulement moyen et turbulent du mercure dans un tube. La méthode aux différences finies de Patankar et Spalding est utilisée pour résoudre les équations paraboliques. Des résultats sont comparés aux mesures antérieures dans un domaine de Ra/Re^2 allant depuis presque zéro jusqu'à 10^{-4}, pour $30\,000 < Re < 90\,000$, et ils prédisent qualitativement les distorsions observées. Des fluctuations de température sont mesurées dans la région de paroi en supplément des expériences précédentes. Les effets du chauffage sur le transfert turbulent d'énergie et de quantité de mouvement sont calculés. Le modèle confirme aussi le renversement mesuré du flux axial turbulent.

TURBULENZMODELLE FÜR MISCHKONVEKTION BEI DER QUECKSILBER-ROHRSTRÖMUNG

Zusammenfassung—Zur Untersuchung des Auftriebseinflusses auf die turbulente Quecksilberströmung in einem Rohr wurde ein einfaches algebraisches Schubspannungsmodell entwickelt. Die Finite-Differenzen-Methode nach Patankar und Spalding wurde zur Lösung der parabolischen Strömungsgleichungen herangezogen. Die Ergebnisse wurden mit früheren Messungen für einen Bereich von Ra/Re^2 zwischen nahezu 0 und 10^{-4} für $30\,000 < Re < 90\,000$ und mit qualitativ beschriebenen, beobachteten Störungen verglichen. In Wandnähe wurden Temperaturschwankungen gemessen, um frühere Messungen zu bestätigen. Einflüsse der Beheizung auf den turbulenten Energie- und Impulstransport wurden vorhergesagt. Das Modell bestätigt ebenso den gemessenen Umschlag der turbulenten axialen Strömung.

МОДЕЛИРОВАНИЕ ТУРБУЛЕНТНОСТИ В СМЕШАННОЙ КОНВЕКЦИИ ПРИ ТЕЧЕНИИ РТУТИ В ТРУБЕ

Аннотация—Для изучения влияния архимедовой силы на осредненное поле и турбулентные характеристики течения ртути в трубе используется упрощенная алгебраическая модель для тензора рейнольдсовых напряжений. Метод конечных разностей Патанкара и Сполдинга применялся для решения модельных параболических уравнений. Результаты сравнивались с ранее выполненными в диапазоне Ra/Re^2 от 0 до 10^{-4} для $30000 < Re < 90000$. С целью дополнения ранее выполненных экспериментов были измерены пульсации температуры в пристенной области. Рассчитано влияние нагрева на турбулентный перенос энергии и количества движения. Моделирование подтвердило также измеренное изменение направления турбулентного потока тепла в осевом направлении.